Stability of Zener order in martensite: an atomistic evidence

Philippe Maugis, Damien Connétable, Paul Eyméoud

Stability of Zener order in martensite: an atomistic evidence

Philippe Maugis [a,*], Damien Connétable [b], Paul Eyméoud [a]

[a] Aix Marseille Univ, CNRS, IM2NP, Marseille, France
[b] CIRIMAT, UMR 5085, CNRS INP UPS, ENSIACET 4, allée Émile Monso, BP 44362, F-31030 Toulouse Cedex 4, France

ARTICLE INFO

Keywords:
Steels
Long-range ordering
Elastic behaviour
Density functional theory (DFT)
Mean-field modelling

ABSTRACT

Martensite is a supersaturated solid solution of carbon in body-centered iron wherein interstitial carbon atoms preferentially occupy a single octahedral sublattice. Despite a century of research, the mechanism of this long-range ordering is still a subject of debate. Recently, Zener's theory of ordering was challenged both experimentally and theoretically. In an attempt to settle the controversy, we investigated by density functional theory the ground states of Fe-C configurations having various degrees of order. We conclude that the fully Zener-ordered configurations are always the most stable energetically, thus confirming Zener's theory. Comparison with mean-field elasticity and Ising-type modelling supports the elastic origin of Zener ordering.

Fink and Campbell in 1926 [1] established that α'-martensite is a supersaturated solid solution of carbon in body-centered iron. The carbon atoms preferentially occupy the octahedral interstitial positions between nearest iron atoms in one of the three ⟨001⟩ crystal directions. This preferential occupation causes a tetragonal distortion of the matrix, quantified by the lattice parameter ratio $c/a > 1$. Based on Bain's transformation, Kurdjumov and Sachs [2] suggested that carbon distribution in martensite lattice inherits from the diffusionless face-centered to body-centered structural transformation of the parent austenite phase. Assuming that long-range carbon–carbon interactions are predominantly elastic, Zener [3] stated that the ordered distribution of carbon atoms is energetically more favorable than disorder. He predicted an order-disorder transition between cubic ferrite and tetragonal martensite (Fig. 1). Zener's mean-field theory has been challenged ever since, partly because the so-called Zener ordering transition was never evidenced directly.

Kurdjumov et al. [4] provided indirect proof of Zener ordering: they measured an increase in tetragonality of quenched martensite during ageing at room temperature, interpreted as progressive ordering via carbon jumps into the favoured octahedral sites. Recently, an in situ X-ray diffraction study of martensite formation during quench evidenced the set up of tetragonality as soon as martensite forms, confirming Bain's scheme [5]. In another study, in situ neutron diffraction revealed a decrease in axial ratio towards $c/a = 1$ during ageing after quench [6], i.e. a case of Zener disordering. Finally, cases were reported of high-carbon austenite isothermally transformed into cubic martensite, thus challenging Zener's model [7,8]. On the other hand, room-temperature measurements of the lattice parameters of Fe-C steels of various carbon contents all show an abrupt transition between low-carbon cubic ferrite and high-carbon tetragonal martensite [9–11], which is coherent with Zener's theory.

On the theoretical side, investigations of carbon ordering in iron involved various techniques: thermodynamic mean-field modelling [12–16], the microscopic elasticity theory [4,10,17–19], the CALPHAD formalism [20,21], molecular dynamics [14,22–24] and combined ab initio–Monte Carlo [16,25–27]. Most of these approaches, although based on different hypotheses and approximations, provide results in favour of Zener ordering. One exception is the work of Ruban [25,26], which predicts an "anti-Zener" ordering consisting of carbon atoms occupying specific sites on *two* preferred octahedral sublattices, associated with a ratio $c/a < 1$. The relative stability of this configuration, as compared to Zener order, is explained by the asserted dominating effect of carbon–carbon short-range interactions.

It is worth noting that mechanical external conditions affect the phase stabilities (see e.g. [28,29]) and modify the equilibrium order. In particular, coherency stress or applied stress can turn the first-order Zener transition into a continuous transition [12,30]. When compressive, a uniaxial stress may also stabilise "beyond-Zener" order, i.e. an orthorhombic structure where the *three* octahedral sublattices are unevenly occupied by carbon atoms [30–33].

This literature survey leads to the conclusion that Zener ordering may or may not occur, depending on yet unclear reasons.

* Corresponding author.
E-mail addresses: philippe.maugis@im2np.fr, philippe.maugis@univ-amu.fr (P. Maugis).
URL: http://www.im2np.fr (P. Maugis)

https://doi.org/10.1016/j.scriptamat.2020.113632

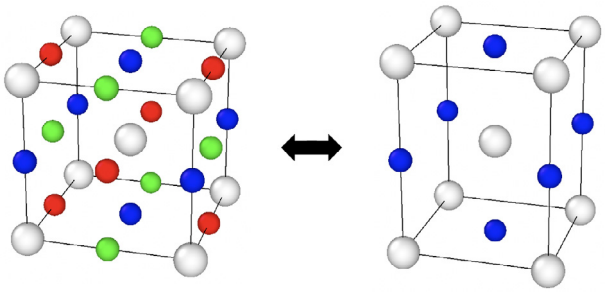

Fig. 1. The Zener order-disorder transition transforms bcc-ferrite (left) into bct-martensite (right) and vice-versa. Fe atoms are in gray, preferred carbon sites are coloured according to their sublattice (RGB code).

Moreover, there is no theoretical consensus on whether Zener order is the most stable state of order in supersaturated iron or not. The subject needs further prospection, given its importance in understanding and predicting the mechanisms of martensite transformation and the resulting martensitic microstructures.

In this study, we investigated from first principles the energetic stability of various states of carbon order. Special quasi-random structures (SQS) were used to simulate random distributions of carbon atoms over each sublattice. Density functional theory (DFT) computations were performed under prescribed applied stress. The results were compared to the mean-field elastochemical model [33] supplemented by short-range carbon–carbon interactions. The most stable structures were identified as function of the applied stress.

In a crystal of body-centered iron, interstitial carbon atoms are distributed over the 3 sublattices of octahedral sites. Carbon fraction on sublattice i is noted c_i and total carbon fraction is $c = \sum c_i$. To study the effect of carbon distribution over the sublattices at constant carbon fraction c, it is convenient to introduce two long-range order parameters η and ζ defined by $c\eta = c_3 - \frac{1}{2}(c_1 + c_2)$ and $c\zeta = c_2 - c_1$. Parameter η quantifies the degree of Zener order along crystal direction [001], while ζ quantifies the unequal occupancy in directions [100] and [010]. In the mean-field approach, a state of order is characterised by the pair of parameters (η, ζ). The case (1,0) represents full Zener order along direction [001], i.e. all carbon atoms sitting on sublattice 3. This configuration will be referred to as the Z3 orientational variant. The combinations $(-0.5, -1)$ and $(-0.5, 1)$ describe the Z1 and Z2 fully ordered variants along directions [100] and [010], respectively. Intermediate values of (η, ζ) represent partially ordered structures. Among them, $(-0.5, 0)$ is the inverse-Zener order: it has empty sublattice 3 and equal occupancy of sublattices 1 and 2. Finally, (0,0) is the fully disordered structure with equal occupancy of the three sublattices.

The thermodynamical stability of a given state of order under applied stress tensor $\boldsymbol{\sigma}$ is characterised by the enthalpy of ordering $\Delta H(\eta, \zeta)$, where symbol Δ expresses that the disordered state is taken as reference. ΔH can be calculated from the energy of ordering ΔU and the strain of ordering $\Delta \boldsymbol{\varepsilon}$ via the relationship

$$\Delta H = \Delta U - V \boldsymbol{\sigma} \cdot \Delta \boldsymbol{\varepsilon}, \qquad (1)$$

where V is the volume of the stress-free carbon-free crystal.

DFT calculations are known to render correctly the short-range interactions between solute atoms, irrespective of their origin, "chemical" or "elastic". In this study, by allowing the supercell to relax, we also captured the long-range carbon–strain interaction and the resulting homogeneous strain.

In order to represent carbon–vacancy disorder on octahedral interstitial sublattices, we used the SQS approach. Supercells were built with mcsqs [34] modulus of ATAT code [35], following the procedure described in [36]: computation of the correlations functions on clusters containing C–C pairs equal to or shorter than $\sqrt{3}a_0$ (a_0 is the lattice parameter of iron). The computed tetragonality and energy somewhat depend on the relative positions of the carbon atoms in the supercell [37,38]), this is why we averaged each case over a set 13 SQS structures. To extract energetic and structural properties from these structures using DFT, we employed an in-house version of VASP code [39,40] allowing to impose stresses on cells. We used the following parameters: generalized gradient approximation [41] with projector augmented wave method [42] and Perdew-Burke-Ernzerhof exchange-correlation functional [43,44], 400 eV energy cut-off (as used in Refs. [36,45,46]), spin-polarized approximation, 10^{-5} eV energy convergence criterion of the electronic self-consistency, $4 \times 4 \times 4$ Monkhorst-Pack k-points grid [47] for 128 iron atom supercells and Methfessel-Paxton smearing [48] for reciprocal space integration. To relax the supercells we used a conjugate-gradient algorithm with ionic relaxation criterion of 10^{-4} eV in energy for zero-stress calculations and 0.01 eV/Å in force for stress-imposed calculations. Calculations were performed on $Fe_{128}C_{12}$ supercells of composition Fe-8.6at%C and varying states of order.

In a first series of calculations, the degree of Zener order along axis 3 was varied (η variable and ζ fixed to zero). Profiles of the averaged ordering enthalpy ΔH and lattice parameters a and c are drawn in Fig. 2. The energetic stability of full Zener order with re-

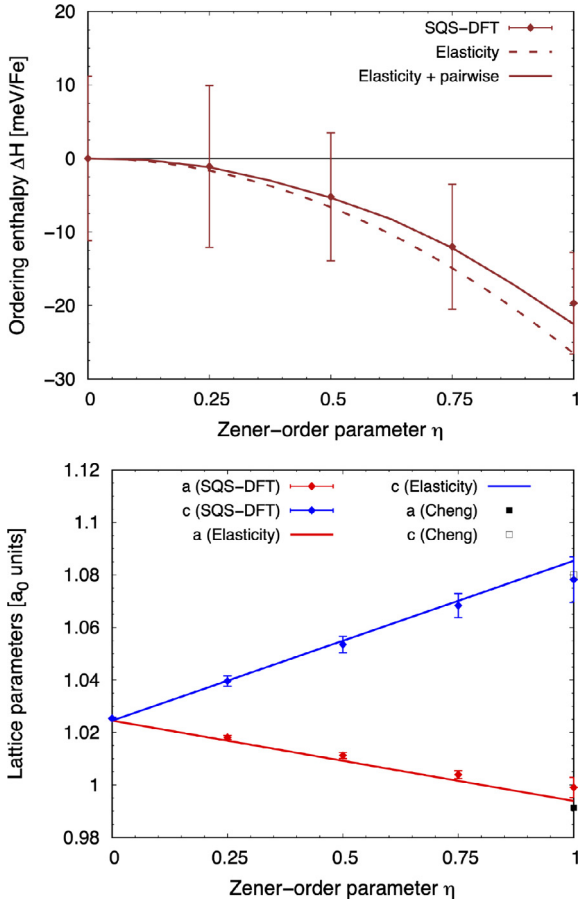

Fig. 2. Ordering enthalpy (top) and lattice parameters (bottom) as function of Zener-order parameter η ($\zeta = 0$) in stress-free Fe-8.6at%C. SQS-DFT is compared to elasticity and pairwise interactions and to experimental data from Cheng [49]. Error bars indicate the standard deviations.

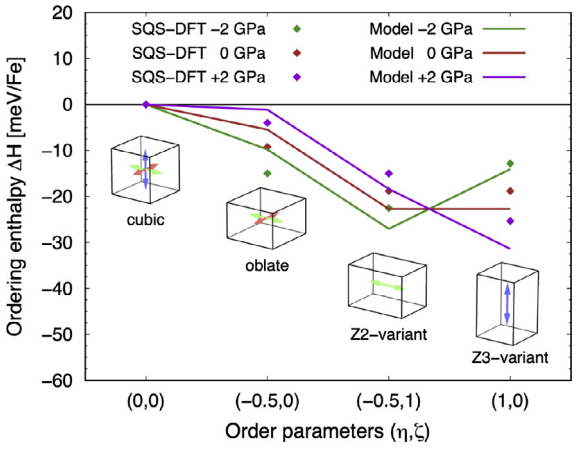

Fig. 3. Ordering enthalpy of various states of order under tensile or compressive stress in Fe-8.6at%C and schematics of the relaxed cell shape (arrows represent the state of order). Fully Zener-ordered configurations are the most stable ones in all cases.

spect to partial order or disorder is evidenced by the minimum in enthalpy positioned at $\eta = 1$. Correlatively, the lattice parameters a and c vary linearly with the order parameter. They reach the experimental values of Cheng et al. [49] at $\eta = 1$, letting assume full Zener ordering for the experimental data collected in this study.

A second series of calculations aimed at investigating the effect of tension (+2 GPa) and compression (−2 GPa) along axis 3 on the relative stability of selected states of order, namely (1,0), $(-0.5, 0)$ and $(-0.5, 1)$. The comparative plotting of Fig. 3 gives the following results: (i) tension stabilises tetragonal Zener order along the stress axis (variant Z3); (ii) compression stabilises orthorhombic Zener order in a direction transverse to the stress axis (variant Z1 or Z2); and (iii) disorder and inverse-Zener order are disfavoured in all cases.

Additional calculations on variants (0,0) and (1,0) revealed that carbon distribution and applied stress have negligible impact on the magnetic moments (less than 0.02 μ_B/atomic species). This negligible role of Zener order on magnetism suggests that an empirical potential without magnetism would be able to capture the discussed effects on Zener ordering.

Here, the main advantages of our first-principles approach are: (i) it correctly represents interstitial disorder thanks to the use of SQS; (ii) it does not raise an issue of empirical potential representativeness, as it is the case for the embedded-atom method [50] and pairwise interactions models; and (iii) it considers both homogeneous elasticity by lattice deformation and C–C chemical interactions. However, this approach does not easily allow discriminating the long-range elastic contribution from the short-range interaction contribution. To investigate this point, we used the mean-field elastochemical model of Maugis [16,33] together with pairwise C–C interactions. The theory is summarised below.

In the framework of the continuum elasticity theory of point defects, long-range carbon–strain interactions are accounted for via the dipole moment tensor $\boldsymbol{P}$ of interstitial carbon [51,52]. Carbon atoms and axial stress σ induce a relaxed strain tensor $\boldsymbol{\varepsilon}$, whose normal components write as functions of η and ζ:

$$\begin{cases} \varepsilon_{11} &= \dfrac{V_C}{3V_0}c + \dfrac{V_\Sigma}{3V_0}c\left(-\eta - \dfrac{3}{2}\zeta\right) + S_{12}\sigma \\ \varepsilon_{22} &= \dfrac{V_C}{3V_0}c + \dfrac{V_\Sigma}{3V_0}c\left(-\eta + \dfrac{3}{2}\zeta\right) + S_{12}\sigma \\ \varepsilon_{33} &= \dfrac{V_C}{3V_0}c + \dfrac{2V_\Sigma}{3V_0}c\eta + S_{11}\sigma \end{cases} \tag{2}$$

Constants V_0, V_C and V_Σ are respectively the atomic volume of the lattice, the relaxation volume and the tetragonal distortion due to an interstitial carbon. The latter are related to the elastic properties of the defect and the host matrix [16]:

$$\begin{aligned} V_C &= (S_{11} + 2S_{12})(P_c + 2P_a), \\ V_\Sigma &= (S_{11} - S_{12})(P_c - P_a). \end{aligned} \tag{3}$$

P_a and P_c are the two independent components of the dipole moment tensor and S_{ij} are the components of the elastic compliance tensor of the host matrix. It is clear from Eqs. 2 that crystal symmetry is governed by both applied stress and order parameters. Indeed, the Bravais lattice may be either cubic ($\eta = \zeta = 0$, $\sigma = 0$; full disorder), tetragonal prolate (e.g. $\eta > 0$, $\zeta = 0$, $\sigma > 0$; Zener order), tetragonal oblate (e.g. $\eta < 0$, $\zeta = 0$, $\sigma < 0$; inverse-Zener order [26,27]) or orthorhombic (e.g. $\eta \neq 0$, $\zeta \neq 0$; beyond-Zener order [4,30]).

The homogeneous strain contributes to the enthalpy of ordering by the amount ΔH^{el} written as

$$\Delta H^{el} = -h_\Sigma c^2\left(\eta^2 + \frac{3}{4}\zeta^2\right) - \frac{2}{3}V_\Sigma \sigma c\eta \tag{4}$$

where h_Σ is the strain-energy parameter:

$$h_\Sigma = \frac{1}{3V_0}(S_{11} - S_{12})(P_c - P_a)^2. \tag{5}$$

The first term in the r.h.s. of Eq. 4 is the stress-independent ordering energy ΔU^{el}. The second term is the elastic work of the applied stress when the configuration is changed from disorder ($\eta = 0$) to partial order ($\eta \neq 0$). Eq. 4 shows that Zener ordering along direction 3 ($\eta > 0$) is favoured when a tensile stress is applied along that direction ($\sigma\eta > 0$, ΔH^{el} decreases); it is disfavoured when a compressive stress is applied along the same direction ($\sigma\eta < 0$, ΔH^{el} increases).

From Eqs. 3 and 5 we notice that the equilibrium state of order, obtained from minimising function $\Delta H^{el}(\eta, \zeta)$ at given c and σ, does not depend on the elastic stiffness of the host matrix, but only on the deviatoric part of the dipole moment tensor, via the ratio $(P_c - P_a)/V_0$.

All material parameters entering the elasticity model were extracted from high-accuracy DFT calculations. Their values are gathered in Table 1. The dipole moment tensor was computed using the residual stress method [53]: a supercell containing one carbon atom in a bcc-Fe matrix was relaxed, while maintaining the shape and volume of the cell identical to that of carbon-free iron. On account of the carbon insertion, a residual stress $\boldsymbol{\sigma}$ builds up at the cell boundary. The dipole moment tensor $\boldsymbol{P}$ is related to the residual stress by $\boldsymbol{P} = -V\boldsymbol{\sigma}$, where V is the volume of the supercell. Correction of the image forces due to the periodic boundary conditions was applied by varying the supercell size and performing a parabolic fit of the residual stress as function of $1/V$.

Table 1
Lattice parameter a_0 (in nm), elastic compliances S_{ij} (in GPa^{-1}) and dipole moments $P_{a,c}$ (in eV) computed by DFT. Volumes V_0, V_C, V_Σ (in eV/GPa) and strain-energy parameter h_Σ (in eV) used in the elasticity calculations.

a_0	S_{11}	S_{12}	P_a	P_c	V_0	V_C	V_Σ	h_Σ
0.2834	5.55×10^{-3}	-1.91×10^{-3}	9.60	18.88	7.10×10^{-2}	6.56×10^{-2}	6.93×10^{-2}	3.02

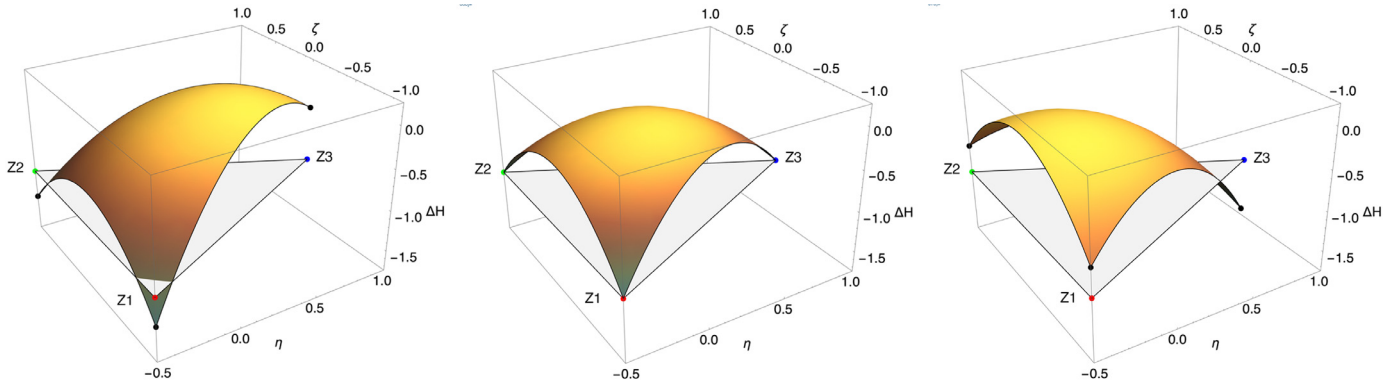

Fig. 4. Ordering enthalpy (in units of $h_\Sigma c^2$) as function of the order parameters η and ζ. From left to right: $\sigma = -1$, 0 and 1 (in units of $h_\Sigma c/V_\Sigma$). The gray triangle drawn at ordinate -1 represents all accessible states of order. Z1, Z2 and Z3 fully-ordered variants (coloured points) are the stable states when no stress is applied (centre). Tension along axis 3 stabilises longitudinal variant Z3 (right), while compression stabilises both transverse variants Z1 and Z2 (left).

Contribution of the short-range carbon–carbon interactions to the enthalpy was written as a pairwise Ising-type model: $H^{\mathrm{nn}} = \frac{1}{2}\sum V_{ij}$, where V_{ij} is the interaction energy between two carbon atoms indexed i and j. The V_{ij}'s were computed by DFT up to the 19th coordination shell [36]. To evaluate $H^{\mathrm{nn}}(\eta, \zeta)$, 250,000 carbon atoms were randomly distributed over the 3 octahedral sublattices according to the specified order parameters and the summation was performed numerically.

The ordering enthalpy computed with the elasticity model coincides well with the decreasing parabolic profile obtained by SQS-DFT (Fig. 2 top), and even better when the C–C pairwise contribution is added. The coincidence remains satisfactory in case of applied stress (Fig. 3): although a slight shift is observed, the influence of the order state is well rendered by the elasticity and pairwise interactions model. We conclude that elasticity captures ∼85% of the ordering enthalpy, while pairwise interactions have a minority contribution of ∼15%. The latter moderate effect is qualitatively in line with the findings of Yan et al. [26]. On the other hand, the influence of ordering on the lattice parameters is perfectly rendered by the elasticity model (Fig. 2 bottom). As expected from elasticity theory, short-range interactions play a negligible role on the carbon-induced homogeneous strain [54].

To generalise our investigation to all possible states of order, surface plots of the reduced ordering enthalpy $\Delta H^{\mathrm{el}}/h_\Sigma c^2$ were computed with the elasticity model for selected values of the reduced applied stress $\sigma V_\Sigma/h_\Sigma c$ (Fig. 4). In the stress-free condition ($\sigma = 0$), ΔH^{el} exhibits three degenerate stable states characterised by the (η, ζ) pairs $(-0.5, -1)$, $(-0.5, 1)$ and (1,0). These pairs represent respectively the fully Zener-ordered variants Z1, Z2 and Z3. We see that when a tensile stress is applied ($\sigma > 0$), the degeneracy is lifted and the stable state is the Zener-ordered variant Z3. In case of compressive stress ($\sigma < 0$) variants Z1 and Z2 are the two degenerate stable states. These variants are oriented transversaly to the applied compressive stress. Owing to the downward concavity of the enthalpy surfaces, all partially ordered states are unstable, including the disordered structure (0,0) and the inverse-Zener structure $(-0.5, 0)$, and this regardless the applied stress.

We have demonstrated that full Zener order is always energetically more favorable than any other state of order, while disorder and inverse-Zener order are unstable. This conclusion is true as long as the carbon atoms are randomly distributed in each sublattice. We did not investigate secondary ordering, i.e. ordering in one or more sublattices, possibly occurring at some specific carbon stoichiometries. Such phenomenon was evidenced experimentally [55] and theoretically [22,25,26,38]. However, secondary ordering is expected to affect only marginally the ordering enthalpies, especially at low-carbon content, thus not invalidating our general conclusions.

Chen et al. reported the experimental evidence of cubic or nontetragonal martensite formed at room temperature in plastically deformed quenched martensite [7], as well as in deformation-induced nanograined martensite [8]. These results apparently contradict our finding that Zener order is expected in martensite, whatever the applied stress. However, the present paper is limited to investigating the 0 K states of a defect-free crystal. At finite temperature, martensite orders on the condition that its carbon content be higher than a critical value. According to literature, this value lies in the range of 0.8 to 2.9 at% at room temperature. Chen et al.'s material may not reach the criterion. Indeed, although their nominal carbon is high, carbon atoms are likely to have migrated to the deformation-induced dislocations and/or to the nanograin boundaries during room-temperature ageing or sample preparation, thus decreasing solute carbon down to a subcritical value.

Our first-principles investigation leads to the conclusion that Zener-ordered configurations of body-centered Fe-C are always energetically favoured compared to disordered or partially ordered ones. This finding supports Zener's theory of ordering. Comparison with mean-field elasticity and Ising-type modelling confirms that Zener ordering is mostly driven by the long-range carbon–carbon strain interaction, while short-range carbon–carbon interactions play a minor role. These conclusions remain true when tensile or compressive stress is applied.

Declaration of Competing Interest

The authors declare that they have no known competing financial interests or personal relationships that could have appeared to influence the work reported in this paper.

Acknowledgements

This work was supported by the Agence Nationale de la Recherche (contract C-TRAM ANR-18-CE92-0021). Centre de Calcul Intensif d'Aix-Marseille is acknowledged for granting access to its high performance computing resources. The authors thank C. Arnold for his technical assistance in compiling the VASP code.

Supplementary material

Supplementary material associated with this article can be found, in the online version, at doi:10.1016/j.scriptamat.2020.113632

References

[1] W.L. Fink, E.D. Campbell, Trans. Am. Soc. Steel Treat. 9 (1926) 717.
[2] G. Kurdjumow, G. Sachs, Zeitschrift für Phys. 64 (5) (1930) 325–343.
[3] C. Zener, Phys. Rev. 74 (6) (1948) 639–647.
[4] G. Kurdjumov, A. Khachaturyan, Acta Metall. 23 (1975) 1077–1088.
[5] J. Epp, T. Hirsch, C. Curfs, Metall. Mater. Trans. A 43 (7) (2012) 2210–2217.
[6] Y. Wang, Y. Tomota, T. Ohmura, S. Morooka, W. Gong, S. Harjo, Acta Mater. 184 (2020) 30–40.
[7] Y. Chen, W. Xiao, K. Jiao, D. Ping, H. Xu, X. Zhao, Y. Wang, Phys. Rev. Mater. 2 (5) (2018) 050601.
[8] Y. Chen, Q. Liu, W. Xiao, D. Ping, Y. Wang, X. Zhao, Mater. Lett. 227 (2018) 213–216.
[9] S. Nagakura, Y. Hirotsu, M. Kusunoki, T. Suzuki, Y. Nakamura, Metall. Trans. A 14A (1983) 1025–1031.
[10] Z. Fan, L. Xiao, Z. Jinxiu, K. Mokuang, G. Zhenqi, Phys. Rev. B 52 (14) (1995) 9979–9987.
[11] O.D. Sherby, J. Wadsworth, D. Lesuer, C. Syn, Mater. Sci. Forum 539-543 (2007) 215–222.
[12] A. Khachaturyan, G. Shatalov, Fiz. Met. Met. 32 (1) (1971) 5–13.
[13] K. Taylor, M. Cohen, Prog. Mater. Sci. 36 (1992) 225–272.
[14] P. Chirkov, A. Mirzoev, D. Mirzaev, Phys. Met. Metallogr. 117 (1) (2016) 34–41.
[15] P. Maugis, F. Danoix, H. Zapolsky, S. Cazottes, M. Gouné, Phys. Rev. B 96 (21) (2017) 214104.
[16] P. Maugis, Acta Mater. 158 (2018) 454–465.
[17] A. Udyansky, J. Von Pezold, V.N. Bugaev, M. Friák, J. Neugebauer, Phys. Rev. B - Condens. Matter Mater. Phys. 79 (22) (2009) 224112.
[18] A. Udyansky, J. von Pezold, A. Dick, J. Neugebauer, Phys. Rev. B 83 (18) (2011) 184112.
[19] X. Zhang, H. Wang, T. Hickel, J. Rogal, Y. Li, J. Neugebauer, Nat. Mater. (2020).
[20] R. Naraghi, M. Selleby, in: P.C. John Allison, G. Spanos (Eds.), 1st World Congr. Integr. Comput. Mater. Eng., TMS, 2011, pp. 235–240.
[21] R. Naraghi, M. Selleby, J. Ågren, Calphad Comput. Coupling Phase Diagrams Thermochem. 46 (2014) 148–158.
[22] C.W. Sinclair, M. Perez, R.G.A. Veiga, A. Weck, Phys. Rev. B 81 (22) (2010) 224204.
[23] P. Chirkov, A. Mirzoev, D. Mirzaev, Mater. Today Proc. 2S (2015) 553–556.
[24] O. Waseda, J. Morthomas, F. Ribeiro, P. Chantrenne, C.W. Sinclair, M. Perez, Model. Simul. Mater. Sci. Eng. 27 (1) (2019) 015005.
[25] A.V. Ruban, Phys. Rev. B 90 (14) (2014) 144106.
[26] J.Y. Yan, A.V. Ruban, Comput. Mater. Sci. 147 (2018) 293–303.
[27] P. Maugis, S. Chentouf, D. Connétable, J. Alloys Compd. 769 (2018) 1121–1131.
[28] O. Shchyglo, T. Hammerschmidt, M. Čak, R. Drautz, I. Steinbach, Materials 9 (8) (2016) 669.
[29] A. Artemev, Y. Jin, A. Khachaturyan, Acta Mater. 49 (7) (2001) 1165–1177.
[30] P. Maugis, J. Phase Equilibria Diffus. 41 (2020) 269–275.
[31] M. Shtremel, F. Satdarova, Fiz. Met. Met. 34 (4) (1972) 699–708.
[32] P. Chirkov, A. Mirzoev, D. Mirzaev, Phys. Status Solidi 255 (7) (2018) 1700665.
[33] P. Maugis, Comput. Mater. Sci. 159 (2019) 460–469.
[34] A. Van de Walle, P. Tiwary, M. De Jong, D.L. Olmsted, M. Asta, A. Dick, D. Shin, Y. Wang, L.Q. Chen, Z.K. Liu, Calphad 42 (2013) 13.
[35] A. Van de Walle, M. Asta, G. Ceder, Calphad 26 (2002) 539.
[36] S. Chentouf, S. Cazottes, F. Danoix, M. Gouné, H. Zapolsky, P. Maugis, Intermetallics 89 (2017) 92–99.
[37] H. Ohtsuka, V.A. Dinh, T. Ohno, K. Tsuzaki, K. Tsuchiya, R. Sahara, H. Kitazawa, T. Nakamura, ISIJ Int. 55 (11) (2015) 2483–2491.
[38] D. Kandaskalov, P. Maugis, Comput. Mater. Sci. 150 (April) (2018) 524–534.
[39] G. Kresse, J. Furthmüller, Comput. Mater. Sci. 6 (1996) 15–50.
[40] G. Kresse, J. Furthmuller, Phys. Rev. B 54 (16) (1996) 11169–11186.
[41] G. Kresse, D. Joubert, Phys. Rev. B 59 (1999) 1758–1775.
[42] P.E. Blöchl, Phys. Rev. B 50 (24) (1994) 17953–17979.
[43] J.P. Perdew, K. Burke, M. Ernzerhof, Phys. Rev. Lett. 77 (1996) 3865–3868.
[44] J.P. Perdew, K. Burke, M. Ernzerhof, Phys. Rev. Lett. 78 (1997) 1396.
[45] L. Ventelon, B. Lüthi, E. Clouet, L. Proville, B. Legrand, D. Rodney, F. Willaime, Phys. Rev. B 91 (2015) 220102.
[46] D. Kandaskalov, P. Maugis, Comput. Mater. Sci. 128 (2017) 278–286.
[47] H.J. Monkhorst, J.D. Pack, Phys. Rev. B 13 (1976) 5188–5192.
[48] M. Methfessel, A.T. Paxton, Phys. Rev. B 40 (1989) 3616–3621.
[49] L. Cheng, A. Bottger, T.H. de Keijser, E. Mittemeijer, Scr. Metall. Mater. 24 (1990) 509–514.
[50] M.S. Daw, M.I. Baskes, Phys. Rev. B 29 (1984) 6443.
[51] D. Bacon, D. Barnett, R. Scattergood, Prog. Mater. Sci. 23 (1980) 51.
[52] R.W. Balluffi, Introduction to elasticity theory for crystal defects, Cambridge University Press, 2012.
[53] C. Varvenne, E. Clouet, Phys. Rev. B 96 (22) (2017) 224103.
[54] A.G. Khachaturyan, Theory of structural transformations in solids, Dover Publications, 2008.
[55] K.A. Taylor, L. Chang, G.B. Olson, G.D.W. Smith, M. Cohen, J.B.V. Sande, Metall. Trans. A 20 (12) (1989) 2717–2737.